Eur. Phys. J. B **39**, 241–247 (2004)
DOI: 10.1140/epjb/e2004-00187-8

THE EUROPEAN PHYSICAL JOURNAL B

A lattice Boltzmann model with random dynamical constraints

A. Lamura[1,a] and S. Succi[2,b]

[1] Istituto Applicazioni Calcolo, CNR, Sezione di Bari, Via Amendola 122/D, 70126 Bari, Italy
[2] Istituto Applicazioni Calcolo, CNR, V.le del Policlinico 137, 00161 Roma, Italy

Received 22 December 2003 / Received in final form 19 March 2004
Published online 29 June 2004 –

Abstract. In this paper we introduce a modified lattice Boltzmann model (LBM) with the capability of mimicking a fluid system with dynamic heterogeneities. The physical system is modeled as a one-dimensional fluid, interacting with finite-lifetime moving obstacles. Fluid motion is described by a lattice Boltzmann equation and obstacles are randomly distributed semi-permeable barriers which constrain the motion of the fluid particles. After a lifetime delay, obstacles move to new random positions. It is found that the non-linearly coupled dynamics of the fluid and obstacles produces heterogeneous patterns in fluid density and non-exponential relaxation of two-time autocorrelation function.

PACS. 47.11.+j Computational methods in fluid dynamics – 05.70.Ln Nonequilibrium and irreversible thermodynamics

1 Introduction

Slow relaxation to local equilibrium is a hallmark of complex system behaviour, with many examples in physics, material science, and biology [1]. From a many-body point of view, the emergence of long-time relaxation seems to be related to the gradual confinement of the system in lower-dimensional regions ('slow' manifolds) of phase-space, surrounded by isolating barriers of increasing amplitude as the temperature is decreased (or density increased) [2]. Within this picture, long-time relaxation is often associated with the appearance of space-time heterogeneities, which can be tentatively attributed to self-trapping effects, i.e. molecules get trapped into 'cages' formed by high-density aggregations of other groups molecules. While the landscape picture necessarily calls for many-body investigations (molecular dynamics, Monte Carlo [3] and various types of lattice-'glasses' [4], for the case of glasses), dynamic heterogeneities can also be interpreted in terms of mutual interactions between fluid molecules of different mobilities [5]. If such a picture is accepted, it is then natural to attempt a description in terms of much simpler effective single-body (mean-field) approaches. This is precisely the conceptual framework of the present work.

We develop a mesoscopic model of dynamically heterogeneous fluids based on the lattice Boltzmann equation (LBE). LBE is a minimal kinetic equation describing stylized pseudo-molecules evolving in a regular lattice according to a simple local dynamics including free-streaming, collisional relaxation and (effective) intermolecular interactions [6]. LBE has proven extremely successful for a variety of complex flows, but its applicability to disordered fluids with long-time relaxation appears more problematic [7]. A crucial ingredient to produce dynamic heterogeneities is (dynamic) geometrical frustration, i.e. the introduction of constraints which reduce the phase-space available to the fluid system. To model these effects, the dynamics of the LBE molecules includes an interaction with space-time dependent obstacles hindering their mobility. As we shall see, the coexistence of 'slow' (the obstacles) and 'fast' (LBE molecules) makes the dynamics of the present model depart significantly from simple fluid behavior.

2 The model

In the present paper, we use a modified lattice Boltzmann equation. Standard LBE with a single relaxation time [8] reads as follows (time-step made unit for simplicity):

$$f_i(\mathbf{r},t) - f_i(\mathbf{r}-\mathbf{c}_i,t-1) = -\omega\left[f_i - f_i^e\right](\mathbf{r}-\mathbf{c}_i,t-1) \quad (1)$$

where $f_i(\mathbf{r},t) \equiv f(\mathbf{r},\mathbf{v}=\mathbf{c}_i,t)$ is a discrete distribution function of particles moving along the direction i with discrete speed $\mathbf{c}_i$. The right-hand side represents the relaxation to a local equilibrium f_i^e in a time lapse of the order of ω^{-1}.

The equilibrium distribution functions f_i^e are expressed as series expansions of the Maxwellian distribution function, up to second order with respect to the local

[a] e-mail: a.lamura@area.ba.cnr.it
[b] e-mail: succi@iac.rm.cnr.it

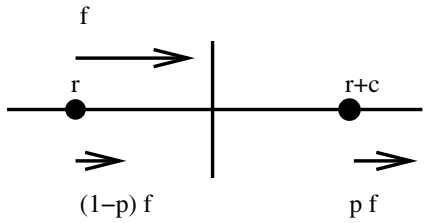

Fig. 1. Schematic representation of dynamical role of obstacles during propagation of distribution functions.

velocity $\mathbf{u}$ [9]:

$$f_i^e = \rho w_i \left[1 + \frac{\mathbf{u}\cdot\mathbf{c}_i}{c_s^2} + \frac{\mathbf{uu}\cdot\left(\mathbf{c}_i\mathbf{c}_i - c_s^2 I\right)}{2c_s^4}\right]. \qquad (2)$$

The local density $\rho = \rho(\mathbf{r}, t)$, as well as the local velocity $\mathbf{u}$ which enter equation (2), are calculated from the distribution functions as follows:

$$\rho = \sum_i f_i, \qquad (3)$$

$$\mathbf{u} = \frac{1}{\rho}\sum_i f_i \mathbf{c}_i. \qquad (4)$$

w_i is a set of weights normalized to unity, c_s the lattice sound speed, and finally, I stands for the unit tensor. In the following, we shall refer to a one-dimensional lattice of size L with $c_i = -1, 0 + 1$ and $c_s = 1/\sqrt{3}$.

We generalize the above equation (1) as follows

$$f_i(r,t) - \left[1 - p(r + \frac{c_i}{2}, t-1)\right] f_i(r, t-1) = p(r - \frac{c_i}{2}, t-1)\Big[f_i(r - c_i, t-1) - \omega\left[f_i - f_i^e\right](r - c_i, t-1)\Big]. \qquad (5)$$

The variables $p(r \pm \frac{c_i}{2}, t)$ live on the lattice links and vary in space and time (non-quenched disorder [10]). We choose them in the form of binary fields taking only the values $p = 1$ and $p = p_t$ with $0 < p_t < 1$. Links with $p = p_t$ act as semi-permeable obstacles which control the propagation rate between neighboring sites in a way which preserves the total density conservation. Figure 1 illustrates in a pictorial way the role of obstacles. Obstacles are characterized by their *permeability*, p_t, and *concentration*, $c = O/L$, O being the number of obstacles, which is kept fixed in time.

The dynamics of the obstacles is the following. At time $t = 0$, the number of obstacles, O, is chosen and their positions are randomly selected. At subsequent times t_n, $n = 1, 2, ...$, where

$$\begin{aligned} t_1 &= \tau_0 \\ t_{n+1} &= t_n + \tau(t_n) \\ \tau(t_n) &= int\left(\tau_0 e^{\frac{1}{2\rho_0}\left(\frac{2}{|m(t_n)-2|}-1\right)}\right) \end{aligned} \qquad (6)$$

the obstacles are shifted rightward to new randomly chosen positions $r_j(t_{n+1}) = r_j(t_n) + r'_j(t_{n+1})$, $j = 1, ..., O$, where $r'_j(t_{n+1}) = int(s) + 1$, s being a random number drawn from an uniform distribution in the range $[\frac{d}{2}, \frac{3d}{2}]$ and $d = \frac{L}{O}$ is the mean inter-obstacle distance. In the above, $int(s)$ denotes the integer part of the variable s. The motion of each obstacle can be seen as a continuous time random walk [11]. In equations (6) τ_0 is the first lifetime and the quantity

$$m(t_n) = (\rho_{max}(t_n) - \rho_{min}(t_n))/\rho_0 \qquad (7)$$

is the relevant order parameter. Here, $\rho_{max}(t_n)$ and $\rho_{min}(t_n)$ are the maximum and minimum values of fluid density at time t_n, respectively, and ρ_0 is the average fluid density. Non zero values of m are the prime indicators of departure from ideal fluid behavior (see below). The quantity τ_0 has to be generally much larger than the time scale of fluid motion so as to characterize obstacles as the slowly moving species of particles. The dependence of τ on the order parameter m is intended to slow down the dynamics of obstacles in the presence of density contrasts (non zero values of m). Indeed, in the expression of $\tau(t_n)$ in (6) it appears a singularity at $m = 2$. The reason is the following. We assumed that, on the average, $\rho_{max} - \rho_0 \simeq \rho_0 - \rho_{min}$ and later numerically verified this assumption to be correct. Since it must be $\rho_{min} \geq 0$, this means that in the limit $\rho_{min} \to 0$ ($\rho_{max} \to 2\rho_0$), namely $m \to 2$, the lifetime of the obstacles must diverge, $\tau(t_n) \to +\infty$.

In moving obstacles we have taken into account the periodicity of the lattice. When a link is already occupied, the moving obstacle is shifted to the nearest neighbor link. The fact that obstacles move rightwards has no effect on the overall fluid dynamics, which depends only on the position of obstacles, and not on their motion. The equation of motion of the obstacles is:

$$p(r + r', t_{n+1}) = p(r, t_n), \qquad n = 1, 2, ... \qquad (8)$$

where the distance r' has been previously defined. Equation (8) is coupled to equation (5) via $\tau(t_n)$, which depends on density through the order parameter $m = m(\rho)$.

Before proceeding further, a few distinguished limits in the phase-plane $p_t - c$ are worth a brief comment:

– *Fluid limit*: Along the lines $c = 0$ (obstacle-free) and $p_t = 1$ (transparent obstacles) the system behaves like a standard LBE fluid.

– *Slow-fluid limit*: Along the line $c = 1$, the system behaves like a standard LB fluid, only with a rescaled speed $p_t u$. Thus, as $p_t \to 0$, this slow fluid goes smoothly into the 'frozen' limit represented by the corner ($p_t = 0, c = 1$), where the system is frozen to its initial configuration.

– *Arrest limit*: Along the line $p_t = 0$ the system is liable to develop density accumulations in a finite time at the locations where the obstacles reside. The actual onset of these density pile-ups depends on the lifetime of the traps, as well as on their concentration. It is in fact clear that dilute obstacles with short lifetimes permit the system to release density pile-ups, thereby avoiding strong

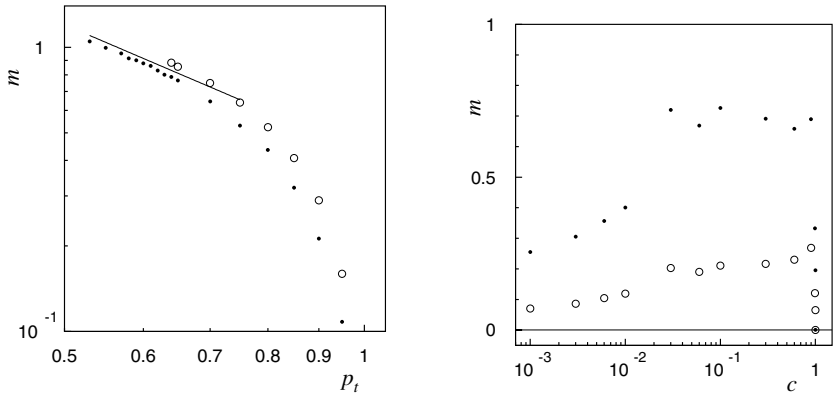

Fig. 2. Left panel: The order parameter m as a function of p_t for different concentrations $c = 0.5$ (•), 0.78 (○). The straight line has slope $-3/2$. Right panel: The order parameter m as a function of c for different values of $p_t = 0.7$ (•), 0.9 (○).

density accumulations. In actual practice, an 'arrest line' of the form $c_A = c_A(p_t, \tau_0)$ marks the upper value of the concentration leading to configurations without accumulation. Intuitively, c_A is an increasing function of p_t and τ_0.

The macroscopic limit of the present model remains an open question mainly because the obstacle populations is generally not smooth, so that a standard Chapman-Enskog analysis is difficult to apply. Here we only present a few remarks which apply to the limit $p_t \to 1$. To leading order in the parameter $1 - p_t$, the main features of density profiles can be explained in terms of the following modified continuity equation:

$$\partial_t \rho + \partial_\alpha (p \rho u) = 0. \tag{9}$$

By writing the above as:

$$\partial_t \rho + \partial_\alpha (\rho u) = -\rho u \partial_\alpha p - (p-1)\partial_\alpha (\rho u) \tag{10}$$

we recognize two extra compressibility terms on the right hand side. The limit $p = 1$ annihilates both extra compressibility contributions, as it must be, since this is the standard LBE situation. The case $p = p_t$ everywhere ($c = 1$), leads again to a standard LBE, only with a rescaled speed $u \to p_t u$, hence no effective extra-compressibility. Genuinely extra-compressibility is therefore associated to spatial changes of the permeability field $p(r,t)$: $\partial_\alpha p \neq 0$ (this derivative must be intended in the sense of distributions, since $p(x,t)$ is generally not smooth).

3 Numerical results

We performed a series of numerical simulations on a lattice with $L = 1024$ grid-points and $\omega = 1.5$. We found that results are not dependent on ω, which was varied in the range $[1, 1.7]$, corresponding to a local collisional relaxation timescale $\tau_c \sim 1/\omega$ approximately in the range $[0.58, 1]$ in time step units. The parameter τ_0 was fixed at $\tau_0 = 50$. The initial condition is $\rho(r) = \rho_0\ (1 + \xi(r))$ where $\xi(r)$ is a random perturbation uniformly distributed in the range $[-0.1 : 0.1]$ and $\rho_0 = 1$.

As a first task, we determine the phase-diagram of our model in the $p_t - c$ plane. We spanned the $p_t - c$ plane and found that departures from ideal fluid behavior ($m \neq 0$) are observed for every value of (p_t, c) with $p_{min} < p_t < 1$ and $0 < c < 1$. The limiting value (arrest value) p_{min} indicates the lowest permeability, below which the simulation is disrupted by excessive density pile-up.

As expected, the arrest value p_{min} decreases with decreasing c: We found $p_{min} \simeq 0.52$ for $c = 0.5$ and $p_{min} \simeq 0.61$ for $c = 0.78$. The behaviors of m as a function of p_t and c are shown in Figure 2. In the vicinity of p_{min}, we observe a power-law behavior $m \sim (p_t - p_{min})^{-a}$ with $a \sim 3/2$. Away from p_{min}, m grows like $(p_{max}(c) - p_t)^b$, with $b \sim 1/2$, which is essentially a mean field theory exponent, and $p_{max}(c) \to 1$ as $c \to 1$. The dependence of the order parameter on c at fixed p_t is non-monotonic, with a kink around $c \sim 0.02$ and a sharp collapse towards the 'slow-fluid' limit, $c = 1$, which appears to be reached in a highly non-perturbative way. To be noted that even a single obstacle $c = 1/L \sim 0.001$ is sufficient to generate sizeable non-zero values of the order parameter m. In summary, these results indicate that fluid behavior is recovered smoothly, but shows very small resilience towards non-zero values of the obstacle concentration c and impermeability $1 - p_t$.

We also considered the dependence of the order parameter m on the lifetime τ_0. Figure 3 shows the behavior of m as a function of the parameter τ_0 in the case with $c = 0.78$, $p_t = 0.7$. It appears that m decays with increasing τ_0 to reach a constant value $m(\infty)$. The reason of this behavior is the following. In the limit of static disorder ($\tau_0 \to \infty$) density profiles are flat among obstacles and show sharp contrasts across them. Density accumulations are prevented in the long time limit by the flow which flattens density among obstacles. When reducing τ_0 it is more difficult for the flow to smooth density profiles and the motion of obstacles produces larger density contrasts in the system as obstacles are shifted thereby causing m to increase. In the limit of rapid motion of obstacles ($\tau_0 \to 0$) it happens that density contrasts are so steep that m diverges. Further simulations with p_t in the range $[0.7, 0.9]$ indicate that that $m(\infty)$ is close to the

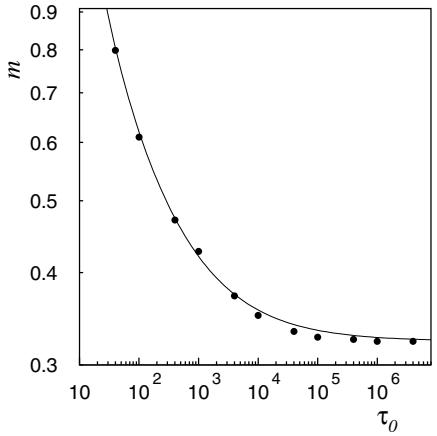

Fig. 3. The order parameter m as a function of τ_0 for $c = 0.78$ and $p_t = 0.7$. The full line is a guide to the eye and represents equation (11).

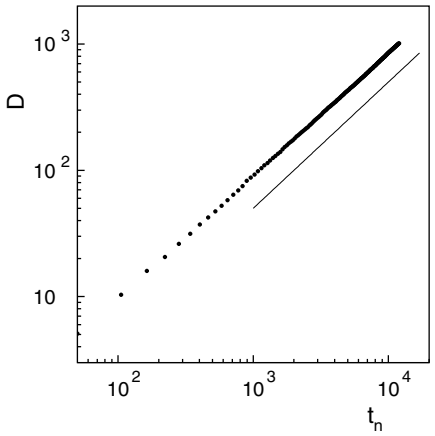

Fig. 4. The distance D travelled by obstacles as a function of times t_n. The straight line has slope 1.

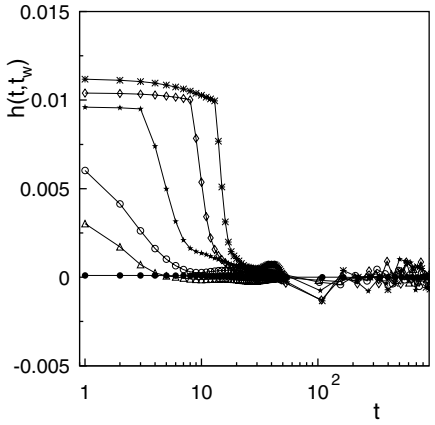

Fig. 5. The density autocorrelation function $h(t, t_w)$ as a function of t for different waiting times $t_w = 1$ ($\triangle$), 52 ($\circ$), 104 ($\star$), 157 ($\diamond$), 211 ($*$). $h(t, t_w)$ is shown also in the case without obstacles for $t_w = 211$ ($\bullet$).

value $(1-p_t)/((1+p_t)/2)$, the latter being an estimate of the density variation across a single obstacle based on the continuity equation (9). It is interesting to observe that the dynamic component of the order parameter m obeys a scaling law of the form

$$\frac{m(\tau_0) - m(\infty)}{m(\infty)} = \frac{a}{(\tau_0 - \tau_{0_{crit}})^{1/2}} \tag{11}$$

again with a mean-field like exponent 1/2, a and $\tau_{0_{crit}}$ being two parameters which depend on p_t.

We next turn to the analysis of the dynamics of the model, notably through a study of the time and space correlation functions. To this purpose, we choose $c = 0.78$, $p_t = 0.7$ and $\tau_0 = 50$ in order to analyse a region of the phase diagram with clear departures from ideal fluid behavior ($m \simeq 0.75$, see Figs. 2–3).

We verified that the resulting motion of obstacles can be described in terms of a directed random walk. Indeed, we have computed the time evolution of the distance D travelled by obstacles defined as

$$D(t_n) = \frac{\sum_{j=1}^{0} r_j(t_n) - r_j(0)}{O}. \tag{12}$$

The quantity D is plotted in Figure 4 as a function of times t_n. From this figure a power law $D \sim t$ is well visible. The exponent 1, characterizing the time behavior of D, is consistent with the fact that the motion of obstacles can be seen as a directed random walk for which the exponent is known to be 1. This result confirms that the obstacle motion is independent on fluid coupling and on obstacle shifting.

We focused our attention on the two-time density autocorrelation function defined as

$$h(t, t_w) = \frac{\langle \delta\rho(r, t_w)\delta\rho(r, t_w + t)\rangle_r}{\langle \rho(r, t_w)^2\rangle_r} \tag{13}$$

where $\delta\rho(r) = \rho(r) - \rho_0$ is the density fluctuation around its spatial average, $\langle ...\rangle_r$ denotes sum over the whole system and $t > t_w$. Multiplying two configurations (one at time t, the other at $t_w + t$) together site by site is sufficient to produce a satisfactory average of $h(t, t_w)$ because, due to the large number of sites ($L = 1024$), the above procedure is equivalent to obtain $h(t, t_w)$ from an ensemble average of the system [12].

The function $h(t, t_w)$ is not normalized to unity at $t = 0$ due to the definition (Eq. (13)). This definition is common for correlations of fluctuations ($\delta\rho$) since small values of fluctuations at the denominator can give diverging contributions to the correlation function itself. The plot for different waiting times is presented in Figure 5. From this figure, evidence of non-exponential relaxation is clearly seen, hinting at the presence of long-lived dynamical structures. Also, the dependence on the waiting time t_w indicates the existence of an underlying non-equilibrium, non-stationary process. In the case without obstacles (standard LBE with $p = 1$ in Eq. (5)) $h(t, t_w)$ is approximately zero (see Fig. 5), as it should be.

Plots of density are shown in Figure 6 in the range 1−500 for a better view. The qualitative behavior is the same over the whole lattice. The corresponding probability distribution functions (PDF) are shown in Figure 7. In the

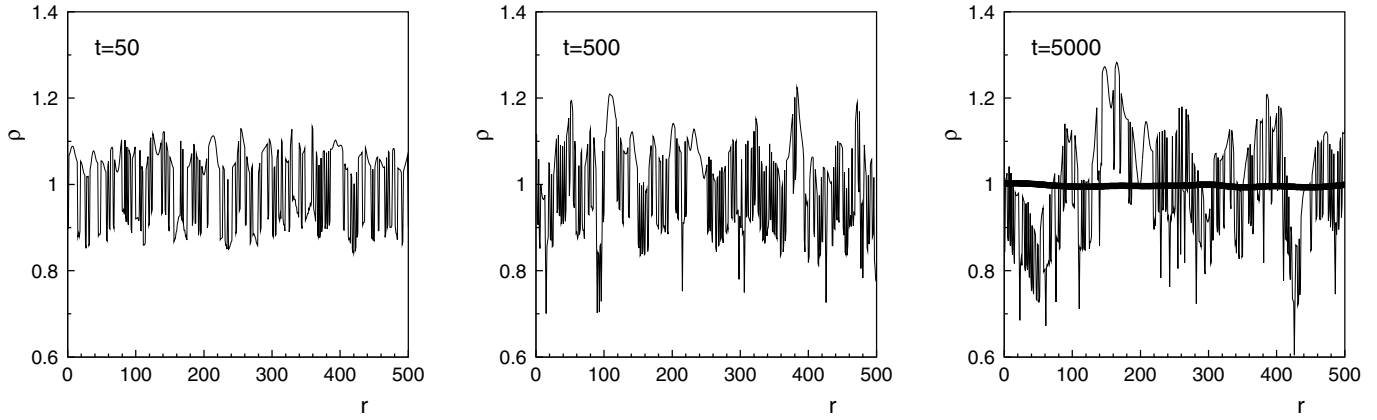

Fig. 6. Density profiles at different times on a portion of the lattice. At time $t = 5000$ the profile is shown also in the case without obstacles (thick line).

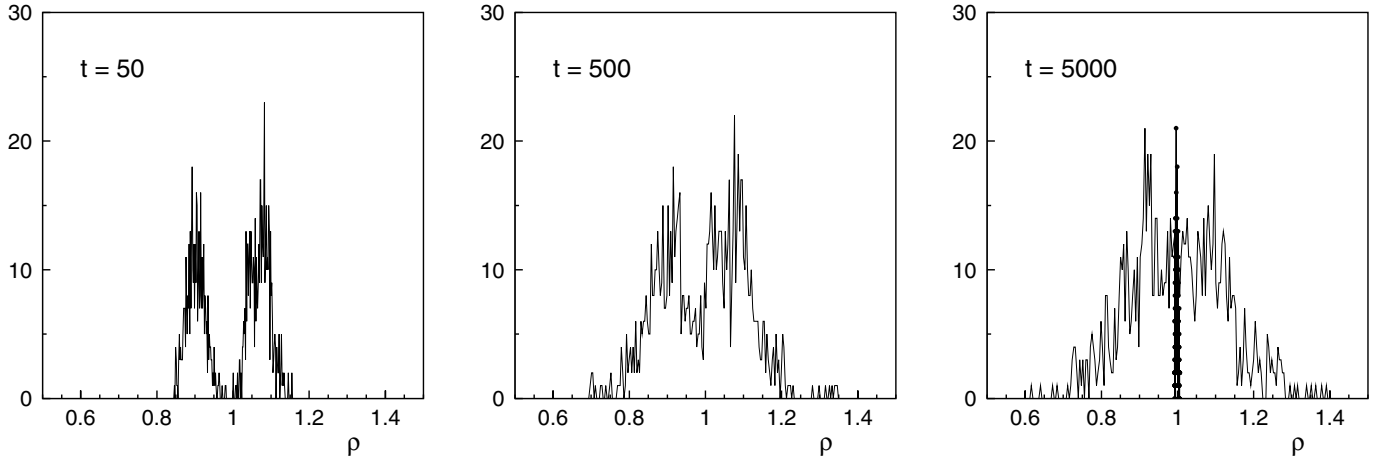

Fig. 7. The probability distribution functions (PDF) of ρ at different times. At time $t = 5000$ the PDF is shown also in the case without obstacles (−●−).

initial stage the PDF quickly forgets the initial distribution and develops two peaks around the initial minimum and maximum densities 0.9 and 1.1 respectively. The apparent phase separation at time $t = 50$ is just due to the effect of obstacles which cause density to accumulate on some lattice sites. Indeed, as soon as the obstacles are released this effect tends to fade away. As time unfolds, these peaks 'diffuse' with the twofold result of filling up the gap at $\rho = \rho_0$ and populating both high and low density tails. It is interesting to note that the PDF generated in these processes are *not* Gaussian, hinting at the presence of (dynamic) heterogeneities in the system. In the case without obstacles density ρ gets constant at value ρ_0 (see Fig. 6 at time $t = 5000$) giving a single peak at $\rho = \rho_0$ in the PDF (see Fig. 7 at time $t = 5000$).

As a further observable, in Figure 8 we plot the density correlation function:

$$g(x) = \frac{\langle \delta\rho(r+x)\delta\rho(r)\rangle_r}{\langle \rho(r)^2\rangle_r}. \qquad (14)$$

From these pictures, the onset of long-range order is well appreciated. In the case without obstacles $g(x)$ is approximately zero (see Fig. 8 at time $t = 5000$).

In order to gain further insights into the dynamics of the density field, we performed a scale-dependent analysis. Let $d\rho(r, x, t) = \rho(r + x, t) - \rho(r, t)$ be the density increment at a scale x at time t, and define the corresponding structure functions as:

$$S_p(x,t) = \langle |d\rho(r,x,t)|^p \rangle_r \,, \qquad p = 1, 2, ..., 5 \qquad (15)$$

as well as scaling exponents a_p via:

$$S_p(x,t) \sim S_p(x_0,t) \left(\frac{x}{x_0}\right)^{a_p}, \quad 1 \le x_0 \ll L \qquad (16)$$

where $x_0 = int(d)$. It is well known that a linear dependence $a_p = Kp$ indicates a fractal process of order K ($K = 1$ for smooth, differentiable processes, $K = 1/2$ for standard diffusion), whereas a non-linear dependence on p would signal a multi-fractal process instead [13]. Our data show that $S_p(x,t) \sim x^{K(t)p}$, where $K(t)$ is a time-varying but scale-independent parameter. This suggests that the density diffusion process is a fractal of dimension $K(t)$, with K raising in the course of the evolution from 0.08 to the steady value 0.15. This also hints at a hierarchical organization of density peaks and dips, which emerges

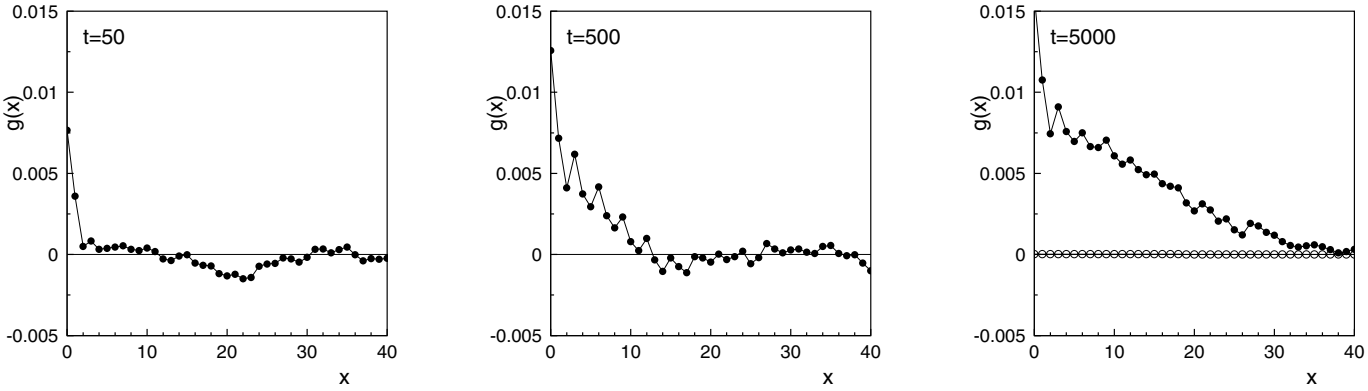

Fig. 8. The density correlation function $g(x)$ as a function of x for different times. At time $t = 5000$ $g(x)$ is shown also in the case without obstacles (○).

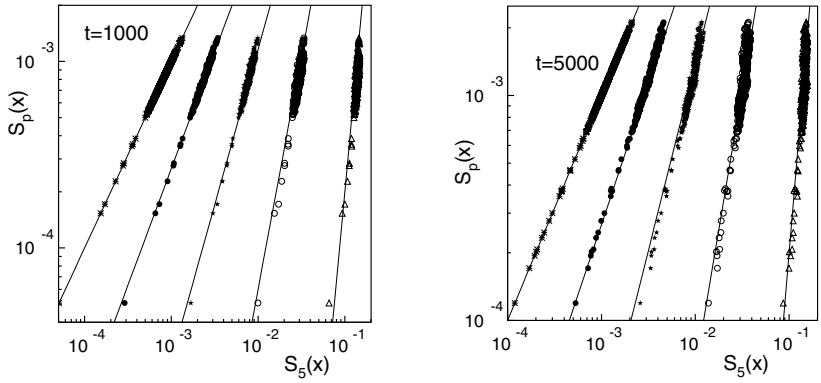

Fig. 9. The structure factors $S_5(x,t)$ as a function of $S_p(x,t)$ for different values of $p = 1$ (△), 2 (○), 3 (⋆), 4 (•), 5 (∗) at two times. The straight line have slopes $5/p$, $p = 1, 2, ..., 5$ from right to left.

spontaneously from the non-linear coupling between the fluid motion and the obstacles dynamics.

The fractal character is more neatly evidenced by using extended self-similarity [14]. Indeed, in Figure 9 we show the plots of $S_5(x,t)$ vs. $S_p(x,t)$ at two times for $p = 1, 2, ..., 5$. Data points fall on the straight lines of slope $5/p$, as expected in the case of fractal behavior. The low values of $K(t)$ indicate that the density redistribution is a *sub*-diffusive process, i.e. it proceeds more slowly than Brownian motion [13], as it is expected for motion in a heterogeneous, disordered background.

4 Conclusions

In summary, we have presented a mesoscopic model of fluid motion with random dynamical constraints. Fluid motion is based on a lattice Boltzmann model, whereas dynamical constraints are implemented via a control field acting as a penetrable barrier for particle motion along the links. Despite its simplicity, our model displays some features of disordered fluids, namely: i) Onset of non-zero order parameter (density contrast) with very small resilience to non-zero obstacle concentration c and impermeability $1 - p_t$; ii) Non-exponential, non-stationary time relaxation of density correlation functions; iii) Long-range spatial order, with non-Gaussian PDF's of the density distribution, iv) Sub-diffusive dynamics of the density distribution.

Although no strict correspondence with any specific physical system can be claimed at this stage, the natural physical target of our model are fluids in porous media with a dynamic morphology, nonlinearly coupled to fluid motion. For the future, we plan to investigate the behavior of the present model for two and three-dimensional fluids. In the long-term, we would also like to model glassy materials, although this is certainly going to require new substantial extensions of the simple model presented in this work.

Illuminating discussions with K. Binder, E. Marinari, G. Parisi and F. Sciortino are kindly acknowledged.

References

1. C.A. Angell, K.L. Ngai, G.B. McKenna, P.F. McMillan, S.W. Martin, J. Appl. Phys. **88**, 3113 (2000); *Disorder effects on relaxational processes,* edited by R. Richert, A. Blumen (Springer, Berlin, 1994)
2. T.S. Grigera, A. Cavagna, I. Giardina, G. Parisi, Phys. Rev. Lett. **88**, 055502 (2002); M.S. Shell, P.G. Debenedetti, E. La Nave, F. Sciortino, J. Chem. Phys. **118**, 8821 (2003)

3. K. Binder, J. Baschnagel, W. Paul, Prog. Polym. Sci. **28**, 115 (2003)
4. W. Kob, H.C. Andersen, Phys. Rev. E **48**, (1993) 4364; G. Biroli, M. Mezard, Phys. Rev. Lett. **88**, 025501 (2002); M. Pica Ciamarra, M. Tarzia, A. de Candia, A. Coniglio, Phys. Rev. E **67**, 057105 (2003)
5. J.P. Garrahan, D. Chandler, Phys. Rev. Lett. **89**, 035704 (2002); R. Richert, J. Phys.: Condens. Matter **14**, R703 (2002)
6. G. Mc Namara, G. Zanetti, Phys. Rev. Lett. **61**, 2332 (1988); F. Higuera, S. Succi, R. Benzi, Europhys. Lett. **9**, 345 (1989); R. Benzi, S. Succi, M. Vergassola, Phys. Rep. **222**, 145 (1992); S. Succi, *The lattice Boltzmann equation* (Oxford University Press, Oxford, 2001)
7. A. Lamura, S. Succi, Physica A **325**, 477 (2003); A. Lamura, S. Succi, Int. J. Mod. Phys. B **17**, 145 (2003)
8. P. Bhatnagar, E.P. Gross, M.K. Krook, Phys. Rev. **94**, 511 (1954)
9. Y.H. Qian, D. d'Humieres, P. Lallemand, Europhys. Lett. **17**, 479 (1992)
10. A.K. Harrison, R. Zwanzig, Phys. Rev. A **32**, 1072 (1985)
11. R. Metzler, J. Klafter Phys. Rep. **339**, 1 (2000)
12. V. Viasnoff, F. Lequeux, D.J. Pine, Rev. Sci. Instr. **73**, 2336 (2002)
13. S. Havlin, D. Ben-Avraham, Adv. Phys. **51**, 187 (2002)
14. R. Benzi, S. Ciliberto, R. Tripiccione, C. Baudet, F. Massaioli, S. Succi, Phys. Rev. E **48**, R29 (1993)